Status and Results of the High-Altitude Water Cherenkov (HAWC) Observatory

R.W. Springer [1*] on behalf of the HAWC Collaboration[2]

[1]University of Utah, Department of Physics & Astronomy, Salt Lake City, Utah, USA

Abstract. The High-Altitude Water Cherenkov (HAWC) Observatory is designed to observe astrophysical sources of cosmic and gamma rays with energies from several hundred GeV up to several hundred TeV. HAWC is a survey instrument that maps a significant fraction of the gamma-ray sky due to its wide field of view. HAWC has extensively studied galactic sources of gamma rays, measuring their energy spectra and morphology. HAWC observes and measures variable and transient sources due to its continuous operation. HAWC has also measured the energy spectrum and anisotropy of the arrival directions of cosmic rays. HAWC participates in multimessenger studies with other observatories, including the Ice Cube neutrino and LIGO/Virgo gravitational wave observatories. HAWC has also performed indirect dark matter searches and studies of beyond-standard model particle physics measurements.

1 Introduction

This article describes the detector and analysis techniques and highlights the scientific results of the High-Altitude Water Cherenkov (HAWC) observatory. The material presented in this article is derived from published journal articles, which can be found on the HAWC website [1]. HAWC was primarily designed to observe the gamma-ray sky, but it has also made significant contributions to studies on cosmic rays, searches for dark matter, and even investigations in solar physics.

2 The HAWC Detector

The HAWC detector, shown in Figure 1, utilizes the Earth's atmosphere as a calorimeter to convert the energy of gamma and cosmic rays into extensive air showers (EAS). These EAS are sampled at the ground by 300 water Cherenkov detectors (WCD) of the densely packed main array [2] and the 345 smaller WCDs of the sparsely packed outrigger array [3] that measure the Cherenkov light produced by the relativistic charged particles. The main array

* Corresponding author: wayne.springer@utah.edu
[2] https://www.hawc-observatory.org/collaboration/

covers an area of approximately 22,000 m^2. It is located at an altitude of 4100 m with a latitude of 180 59' N and a longitude of 970 18' W. The 345 additional outrigger WCDs increase the total footprint of HAWC by approximately a factor of four, albeit with sparser sampling in the periphery. The main-array WCD is a cylindrical metal tank 7.3 m in diameter containing approximately 188,000 liters of purified water. Four upward-facing photomultiplier tubes are installed in each tank to convert the Cherenkov light produced in the water tank into an electrical signal. A time-over-threshold readout system measures the charge and time of these electrical signals. The smaller outrigger WCD tanks are 1.55 m in diameter and 1.65m in height. A single upward-facing Hamamatsu R5912 8" photomultiplier tube samples the Cherenkov light in the outrigger WCDs. A flash analog-to-digital (FADC) readout system digitizes the signals from the outrigger array [4].

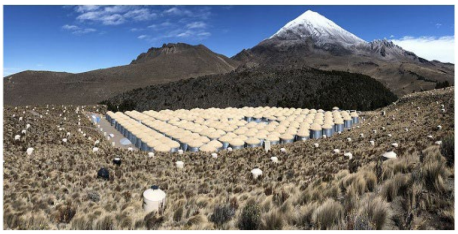

Fig.1. Photograph of the HAWC observatory taken from the base of Sierra Negra with Pico de Orizaba in the background. The 300 large main array WCD tanks are in the center. The smaller tanks seen in the photo are those of the outrigger array.

The arrival direction of the primary particle is reconstructed from the arrival times and locations of the PMT signals. A lateral distribution function of the EAS front is reconstructed from the charge and locations of the PMT signals from which the primary particle's energy is determined. The sensitivity and performance characteristics of HAWC have been determined using simulation software based on Corsika [5] to model the extensive air showers (EAS). HAWC's detector response to the EAS was simulated using the Geant4 [6] software package. Time and charge calibration [2] of HAWC is performed using a hardware-based system to inject laser light pulses into each WCD. Further calibration [7] is obtained from detailed data studies, such as examining time residuals in the extensive air shower data. Data from the Crab Nebula was valuable in validating the performance of HAWC. A study of the energy dependence of the displacement of the Moon's cosmic ray "shadow" due to the Earth's magnetic field provided a mechanism to validate the energy scale of the HAWC measurements.

3 The TeV Gamma Ray Sky – Galactic Results

HAWC observes approximately 2/3 of the sky every 24 hours from -26^0 to +64^0 in declination. In addition to excellent sensitivity to point sources, HAWC has superior sensitivity to extended sources such as Pulsar Wind Nebulae (PWN) and a new class of objects referred to as TeV Halos. The techniques to reconstruct the primary particle's properties are described in the article on the first measurement of the spectral energy distribution of the Crab Nebula [8], shown in the left panel of Figure 2. The right panel of Figure 2 shows a later measurement of gamma-ray emission up to at least 100 TeV

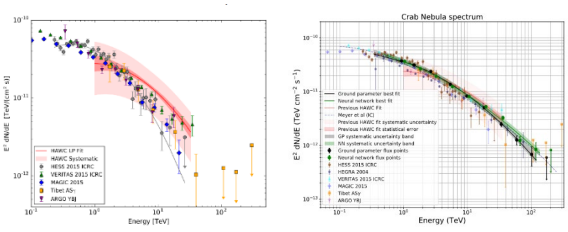

Fig. 2. The left panel shows the spectral energy distribution of gamma-ray emission of the Crab Nebula, first published by HAWC [7]. On the right is a spectral energy distribution of the Crab Nebula, measured by HAWC using a parametric and neural-network approach, showing measured emission up to at least 100 TeV [8].

[9]. Note the improvements in statistical and systematic uncertainties and the improved reach to higher energies above 100 TeV in the later measurement.

HAWC has released its third Catalog of TeV energy scale gamma-ray sources [9]. The sensitivity is somewhat unbiased in time because it continuously observes the sky above the observatory. However, the sensitivity depends on the source's declination and spectral index and flux, which are more sensitive to hard-spectrum sources. Sixty-five sources were observed at a significance > 5 sigma in the 1523-day exposure. The significance calculations were carried out using four different assumptions for source morphology: point-like, shown in Figure 3, and 0.5◦, 1.0◦, 2.0◦ extended sources.

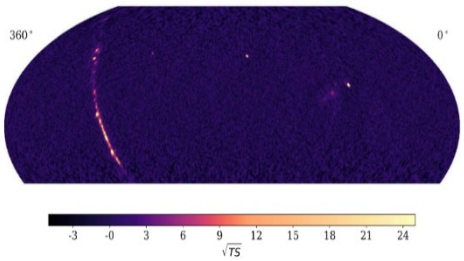

Fig. 3. Celestial coordinate map of the 3rd HAWC Catalog [10]. The galactic plane is seen as a band on the left. The Crab Nebula and the Geminga halo are near the galactic anti-center. The extragalactic sources, Mrk 501 and Mrk 421, can also be seen in the map's upper center.

Pulsar Wind Nebulae, TeV Halo, and Micro-quasar lobe sources are detected at increased significance using extended source assumptions. The ability of HAWC to observe extended sources is illustrated in Figure 4 by the observed extended emission region of Geminga, which extends over several degrees of the sky. Preparation of the fourth Catalog of HAWC sources with greater statistics and improved reconstruction techniques is ongoing.

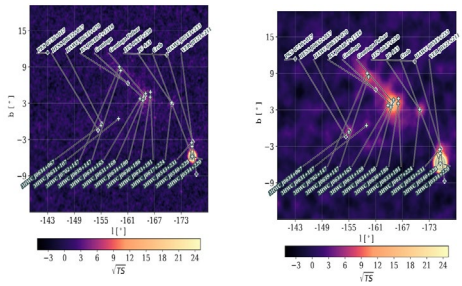

Fig. 4. Sky region near Geminga and the Crab Nebula from the 3rd HAWC Catalog [10]. The significance map assuming a point-source hypothesis is shown in the left panel. The significance map on the right assumes a 1-degree extended source hypothesis.

HAWC [11] and H.E.S.S [12] have observed extended emission regions of TeV gamma rays surrounding pulsars. Theorists [13], [14] have suggested that extended TeV emission regions, dubbed TeV Halos, could be a common feature of pulsars. HAWC's observation of extended emission about the Geminga pulsar [11] has been used to constrain the origin of the anomalous positron flux observed at Earth by cosmic ray detectors such as AMS [15]. HAWC has recently updated its observations of TeV halos about Geminga and Monogem [16]. This observation confirms that local pulsars, such as Geminga, can produce a sizeable part of the positron flux measured by AMS-02 above 10 GeV. HAWC has also observed a TeV halo, shown in Figure 5, associated with PSR J0359+5414 at > 6-

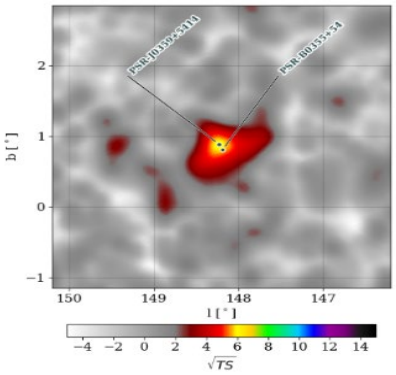

Fig. 5. Significance map in Galactic coordinates showing extended emission TeV halo surrounding the known location of PSR J0538+5414[17].

sigma significance in an exposure of 2321 days [17]. This pulsar is younger, radio-quiet, and in a non-crowded region of the outer galaxy.

HAWC has observed the lobes, shown in Figure 6, of the microquasar SS-433a binary system, comprised of a supergiant star accreting onto a compact object [18]. TeV emission in the lobe regions is observed at > 6-sigma after subtracting the presumed emission from J1908+06. One interpretation for the emission of high-energy gamma rays is the acceleration of charged particles to PeV energies in the microquasar's jets. However, hadronic acceleration is disfavored due to the extreme energetics required. Acceleration does not happen at the black hole because the cooling time of the electrons is too short to make the observed gamma rays.

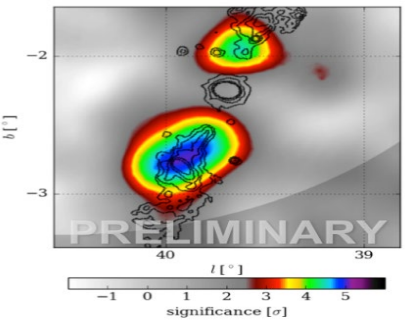

Fig. 6. Lobes of microquasar SS-433 as seen by HAWC [18]. The map shows significance vs galactic coordinates. Note the angular extent of the emission region exceeds 1^0.

With increasing exposure, sources at ever-increasing energies are being detected by HAWC. In 2020, HAWC published an article reporting multiple galactic sources with emissions above 56 TeV detected by HAWC [19]. At that time, about 30 sources above 50 TeV, nine sources above 56 TeV, and three sources, above 100 TeV were observed. Another source of high energy emission above 200 TeV observed by HAWC is J1825-134 [20]. This source is coincident with a Giant Molecular Cloud. It is possible that this very high energy extended source emission is from the collisions of cosmic rays accelerated to energies of several PeV with the ambient gas. The Cygnus Cocoon region's very high energy gamma-ray emission may be due to the collisions of freshly accelerated cosmic rays, as reported by HAWC [21].

Studying the spectral properties of gamma-ray sources aims to ascertain whether the emission is of hadronic origin, thereby identifying the sources of PeV energy galactic cosmic rays. However, detecting gamma rays' high-energy emission is insufficient to claim the origin of hadronic emission. The first LHAASO Catalog reports 43 sources with emission energy above 100 TeV [22]. Several LHAASO UHE sources, including the Crab Nebula, are leptonic accelerators such as pulsars and PWN [23]. LHAASO also reports the observation of photons up to 1.4 PeV [24], although the counterparts responsible for this UHE emission were not identified. Fitting detailed models of the leptonic and hadronic emission mechanisms to measured spectra from joint observations may allow a hadronic interpretation in some cases, such as MGRO J1908+06 [25] observed by HAWC, Fermi-LAT, LHASSO, and XMM-Newton. However, as shown in Figure 7, a definitive conclusion about the acceleration mechanism could not be reached in the HAWC analysis of the

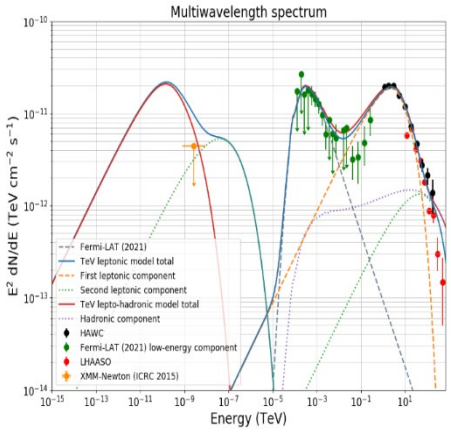

Fig. 7. Leptonic and Hadronic model components fit to measured spectral points of MGRO J1908+06 from HAWC, Fermi-LAT, LHAASO and XMM-Newton measurements [24]. No clear preference for either hadronic or leptonic emission may be concluded or excluded from this study.

multiwavelength spectrum of MGRO J908+06. Recent observations of ultrahigh-energy gamma rays from the Galactic Center by HAWC indicate the presence of a PeVatron accelerating protons to PeV energies there [26]. Further observations with present and planned gamma-ray observatories will further elucidate the nature of this UHE gamma-ray emission. Another promising approach to identifying hadronic emission mechanisms is to perform multimessenger observing campaigns with neutrino detectors, such as the IceCube observatory as mentioned later.

4 The TeV Gamma Ray Sky – Extragalactic Results

Due to its relatively high energy threshold and the attenuation of gamma rays by the extragalactic background light, HAWC reliably observes only two extragalactic sources. Three known very-high-energy extragalactic sources, the radio galaxy M87 and the BL Lac objects VER J0521+211 and 1ES 1215+303, have been observed at a marginal significance, just above the 3σ level [27]. We find evidence for collective emission from 30 stacked extragalactic sources, with Mkn 421 and Mkn 501 excluded, at a significance of 4.2-sigma. The effects of this attenuation on the spectral energy distributions of Mkn 421 and Mkn 501 were used to measure the density of the extragalactic mid-infrared background with HAWC [28].

The HAWC observatory monitors gamma-ray sources daily [29]. Figure 8 shows the integrated flux measurements for each of the ~471 transits of Mkn 421, Mkn 501, and the Crab Nebula between November 26, 2014, and April 20, 2016. The TeV Blazars Mkn 421 and Mkn 501 variability is quite large, as shown in Figure 8. The flux from Mkn 501 has sometimes exceeded three times the flux of the Crab Nebula.

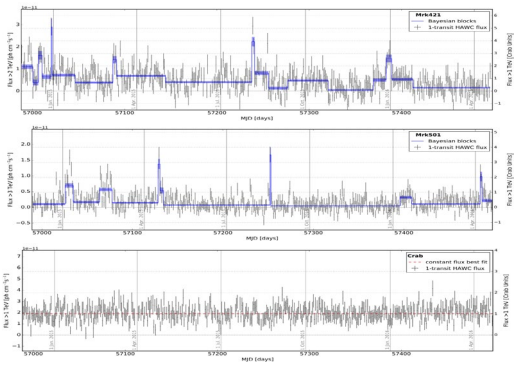

Fig. 8. Integral flux during a transit vs time for Mkn 421 (upper panel), Mkn 501 (middle panel) , and the Crab Nebula (lower panel)[29].

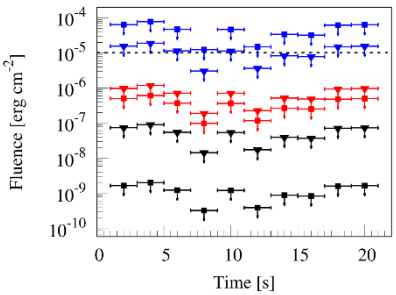

Fig. 9. Spectral-index and redshift-dependent upper limits on the fluence in the energy range 80-800 GeV [32]. Triangles indicate a spectral index of -0.7, squares indicate an index of -2.2, Black indicates redshift=0, red indicates redshift=0.3, and blue indicates redshift=1.0. The dashed line indicates the average flux measured by Fermi-GBM.

HAWC has yet to observe a signal from a GRB. This is due to the energy spectra, distance to most GRBs, and the attenuation of gamma rays due to the EBL coupled with the relatively high energy threshold of HAWC [30]. GRB 221009A had flux and energy spectra that would have been observable by HAWC had it been in its observable sky. GRB 221009A was located overhead of LHAASO, and they could measure the properties of the spectra and flux as reported in [31]. HAWC has examined its data to search for simultaneous or delayed and extended VHE gamma-ray emission associated with a sample of 47 short GRBs. The upper limits obtained from that search [32], are shown in Figure 9.

5 Cosmic Ray Results

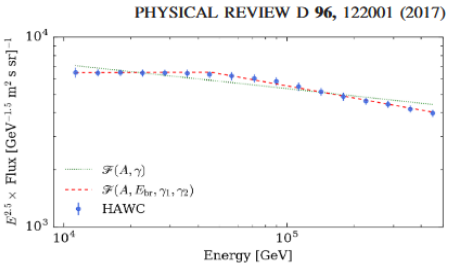

Fig. 10. The all-particle differential energy spectrum scaled by $E^{2.5}$. measured from 8.42 x 10^9 events obtained over a 234-day exposure [32].

A measurement of the all-particle energy spectrum of cosmic rays, shown in Figure 10, based on a 234-day exposure time was published in reference [33]. This measurement used 8.42 x 10^9 events after selection cuts, ensuring well-reconstructed events. The primary energy was determined using a maximum likelihood approach from the particle density as a function of distance to the shower core, lateral distribution function, of the EAS on an event-by-event basis. An energy response matrix, $P(E_{reco}|E)$, was obtained by simulating the detector response, relating true energy to reconstructed energy. The reconstructed energy distribution was unfolded iteratively using probability distributions based on this simulated energy response matrix. Detailed simulations were used to determine $A_{eff}(E)$ and its systematic uncertainties for the applied selection cuts. The HAWC collaboration has completed an update to the all-particle spectrum using a larger data sample. That article is in the final stages of collaboration review and will have been submitted by the time this proceeding is published.

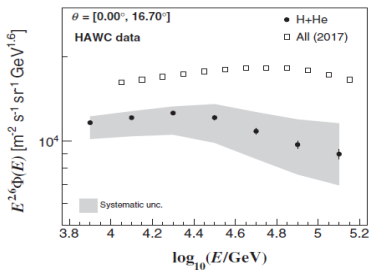

Fig. 11. The energy spectra of proton plus Helium (black dots) compared to all-particle cosmic rays (box) [33]. The error bars represent statistical uncertainties, and the gray band represents systematic uncertainty.

A measurement of the differential energy spectrum of primary protons and helium based on data collected between June 2015 and June 2019 was published in reference [34]. The event sample was enriched in protons and helium by applying a selection cut on the lateral age of the air shower. The lateral age of iron-induced air showers is significantly higher on average than air showers induced by lighter elements, proton, and helium. This energy-dependent selection cut was determined using Corsika with the QGSJET-II-04 hadronic interaction model. This measurement found that the proton-plus-helium spectrum is consistent with a broken power law with an index of −2.51 +/-0.02 prior to a break at 24.0 +3.6/- 3.1 TeV, followed by an index of −2.83 +/- 0.02, where the quoted uncertainties are statistical.

Figure 12 shows the large and small-scale anisotropy in arrival directions measured over almost the entire sky by HAWC and IceCube [35]. The combined map eliminates bias in the angular power spectrum resulting from partial sky coverage. The large-scale anisotropy, described mainly by a dipole, is in the left panel. After subtracting the dipole distribution, the small-scale anisotropy is obtained and shown in the right panel of Figure 12.

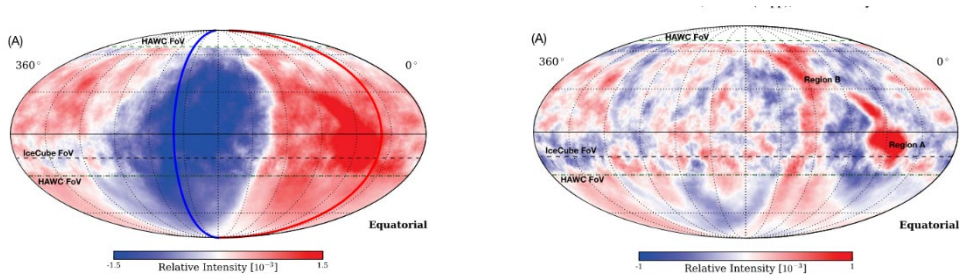

Fig. 12. Left Panel: Relative intensity showing dipole nature of the large-scale anisotropy in arrival directions of cosmic rays. Right Panel: Relative intensity showing small-scale anisotropy [34].

6 Other Contributions and Future Plans

HAWC has participated in joint observing programs with many other observatories spanning the electromagnetic spectrum. Additionally, multimessenger campaigns with gravitational wave and neutrino observatories contribute to our understanding of the Universe. As mentioned in the section on the search for the origin of cosmic rays, the IceCube observatory has searched for neutrino candidates associated with potential cosmic ray acceleration sites [36]. HAWC has performed follow-up searches for gamma-ray emission from the gravitational wave sources detected by LIGO and VIRGO [37]. The lack of space has precluded discussion of many topics, including searches for dark matter [38], test of Lorentz invariance violation [39], and several solar physics studies [40].

A large contingent of the HAWC collaboration is joining with other particle astrophysicists worldwide to construct a large high-altitude gamma-ray observatory, known as the Southern Wide-Field Gamma-Ray Observatory (SWGO) [41], at a site located at 4770m in Chile. This detector will eventually be significantly larger than HAWC, resulting in greater sensitivity at higher energies. The higher altitude will improve low-energy sensitivity. Perhaps most importantly, SWGO will have a better view of the Southern Sky, including the Galactic Center.

References

1. https://www.hawc-observatory.org/publications/#articles
2. Abeysekara et al., *NIMA* 1052:168253. (2023)
3. Marandon V., *et al.*, Proc. Sci., 358 (2021), p. 7361-8.
4. Puehlhofer, G.,et al. 2015, 34th (ICRC2015), 1039v
5. D. Heck et al., FZKA-6019 (1998)
6. Agostinelli, S. , *et al*., *NIMA*,**506**, Issue 3,(2003).
7. Albert *et al* 2024 *ApJ* **972** 144*v*
8. Abeysekara, A.U.,*et al.,*ApJ **843** 39 (2017).
9. Abeysekara, A.U., *et al.*, ApJ**881**(2019), 134.
10. A. Albert et al. 2020, ApJ **905** (2020) , 76.
11. Abeysekara, A. U.,*et al.* . *Science*. https://doi.org/aan4880*v*
12. Abdalla, H.,et al. 2018, Astron. Astrophys., 612, A2v.
13. Linden et al. 2017. Phys. Rev. D **96**, 103016

14. Linden & Buckman 2018 Phys. Rev. Lett., 120, 121101.
15. Accordo,L. , *et al.* , Phys. Rev. Lett. **113**, 121101 2014
16. Albert *et al* 2024, *ApJ* **974** 246
17. A. Albert et al., ApJL **944** (2023) , L29 .
18. Abeysekara, A.U. et al., Nature **562** (2018) , 82-85.
19. A.U. Abeysekara, A.U. et al., PRL **124**,021102(2020) .
20. Albert, A., et al. 2021, ApJL **907** (2021) , L30.
21. A. Albert et al., Nature Astron (2021).
22. Cao, Z., *et al* 2024 *ApJS* **271** 25
23. Cardillo, M., & Giuliani, A.. *Applied Sciences, 13*(11), 6433.
24. Cao, Z. *et al.*, *Nature* **594**, 33–36 (2021)
25. Albert, A. *et al* ,2022 *ApJ* **928** 116.
26. Albert, A. *et al*., 2024 *ApJL* **973** L34
27. Albert, A. *et al* 2021 *ApJ* **907** 67
28. A. Albert, A. et al. 2022, ApJ **933** (2022) , 223..
29. Abeysekara, A. U. et al., ApJ 841 (2017) , 100.
30. Abeysekara, A.U. et al., Astropart. Phys. **35** (2012) 641-650.
31. Cao, Z., et al., *Science* **380** 6652 (2023)
32. Albert, A. et al. 2022, ApJ **936** (2022) , 2.
33. Alfaro, R. et al., Phys. Rev. D 96 (2017) , 122001
34. Albert, A. et al. 2022, PRD **105** (2022) , 063021
35. Abeysekara, A.U. et al., and Aartsen, M.G. et al., ApJ871(2019) , 096.
36. The IceCube, Fermi-LAT, MAGIC, AGILE, ASAS-SN, HAWC Collaborations, etc., Science 361 (2018) , 146-155
37. LIGO Collaboration, Virgo Collaboration, HAWC Collaboration, etc., ApJ **848** (2017)
38. Albert, A. et al., ApJ **853** (2018) , 154.
39. Albert, A. et al., PRL **124**,021102(2020) .
40. Alfaro, R. et al. 2024, *ApJ* **966** 67
41. Abreu, P., et al. arXiv:1907.07737v